Front. Earth Sci. 2015, 9(3): 509–520
DOI 10.1007/s11707-015-0491-x

RESEARCH ARTICLE

A three-dimensional modeling of the morphological change in the Liaodong Bay

Qiushun WANG (✉), Haigui KANG

State Key Laboratory of Coastal and Offshore Engineering, Dalian University of Technology, Dalian 116024, China

Abstract The morphology in the Liaodong Bay has undergone a marked change over the past decades due to the cutoff of nearby rivers. The fine sediment of the bay consists of both non-cohesive and cohesive fractions with relatively small particles over the seabed. Thus, a three-dimensional morphodynamic model accounting for non-cohesive and cohesive fractions is established to investigate the morphological change without sediment input from nearby rivers. A representative wave is chosen to compute the wave distribution in the Liaodong Bay and depth-dependent wave radiation stresses are employed by the hydrodynamic model. The advection-diffusion equation is used to simulate the fine sediment transport under the representative wave and tidal currents. The erosion flux of non-cohesive and cohesive sediment is taken into account. The simulated results of tidal level, velocities, directions, and sediment concentrations are in agreement with the measured data. The results demonstrate that the present model, which takes the erosion flux of both non-cohesive and cohesive fractions into account, gives more reasonable values than when accounting for cohesive sediment alone. When the three-dimensional morphodynamic model is applied to predict morphological change over the course of a year, the deposition is shown to be relatively small and the range of the erosion is increased compared to previous results of sediment input from the river. It can be concluded that the erosion in the Liaodong Bay is increasing due to the cutoff of the river, and that morphological evolution must be taken into account if any type of coastal construction plans are to be carried out over the seabed.

Keywords fine sediment, three-dimensional model, morphological change, representative wave

1 Introduction

In recent years, the topography of the Liaodong Bay, located north of the Bohai Sea, has changed due to a decease of sediment input from nearby rivers (Wang et al., 2010). Morphological changes in the bay have been previously studied by comparing historical charts and measuring the decay characteristics of the metallic element (Wang and He, 1993; Fu et al., 1994; Miao et al., 1996). Additionally, sediment suspension investigations were carried out by remote sensing (Zhang et al., 2011; Pang and Yu, 2013), which focused on the large-scale distribution of sediment concentration over the surface layer. However, there are few numerical studies of the morphological change in the Liaodong Bay. The seabed in the coastal waters of the bay is composed of fine sediment, which is comprised of both non-cohesive and cohesive fractions. Non-cohesive sediment is characterized by its uniform, grain-size distribution, whereas cohesive sediment is influenced by electrochemical and biologic cohesion. The fine sediment transport is related to the currents and sediment concentrations, of which the vertical distribution is depth-dependent. Meanwhile, the morphological change in the horizontal domain is non-uniform. Consequently, these features are more accurately described by a three-dimensional model.

Much effort has been devoted to the development of three-dimensional morphodynamic models to resolve all scales for non-cohesive or cohesive sediment. Authors have previously studied the sediment types separately. Since the concept of erosion fluxes was proposed, the cohesive sediment transport has been solved by the advection and diffusion equation under the explicit definition of the source term (Lopes et al., 2006; Chao et al., 2008; Du et al., 2010; Xie et al., 2010). Some authors used the erosion flux to study non-cohesive sediment transport (Lin and Falconer, 1996; Warner et al., 2008; Pinto et al., 2012). Minimal research that simultaneously involves both classes of sediment has been conducted due

Received April 2, 2014; accepted August 31, 2014

E-mail: wangqsh1015@mail.dlut.edu.cn

to the difficulties raised by the complex interactions between cohesive and non-cohesive sediment. Waeles et al. (2007) applied a formulation of erosion fluxes to resolve the transport of mixed sediment. Le Hir et al. (2011) gave a strategy for mixed sediment in sediment transport modeling. The median diameter of mixed sediment in the Liaodong Bay is small, and the advection-diffusion equation can be reasonably used since fine sediment is mainly transported in suspension. Therefore, the investigation of fine sediment over the seabed by the advection and diffusion equation under the erosion flux of mixed sediment is essential.

Application of morphodynamic models spanning a longer time in large-scale zones has been challenged due to the interactions between waves, currents, and sediment. The net change over one tidal cycle is small, although the amount of sediment being transported may be large in coastal zones. As a consequence, it becomes increasingly important to predict the yearly morphodynamics in order to evaluate the net change. For longer time scales, the morphodynamic model monitors the net erosion and deposition over the seabed. However, fully-coupling models over a long duration will be computationally expensive. Some strategies were proposed by Lesser et al. (2004) and Roelvink (2006) in an attempt to deal with the dilemma between the short-term hydrodynamic processes and long-term morphological changes. To minimize computation time, the concept of representative tides and waves was proposed (Chesher and Miles, 1992; de Vriend et al., 1993; Latteux, 1995). The use of this concept in morphodynamic models effectively reduces the calculation time for each loop. Chonwattana et al. (2005) employed representative waves in the morphological model to calculate large-scale morphology. It will undoubtedly be useful to employ representative waves in practical applications.

The objective of this study is to develop a three-dimensional morphodynamic model to resolve the morphological change without sediment input from the river in the Liaodong Bay. Based on the three-dimensional circulation model FVCOM (Finite Volume Coastal and Ocean Model), a morphodynamic model including cohesive and non-cohesive sediment is developed. The fine sediment consists of cohesive and non-cohesive content, and has a median diameter of 0.0157 mm. Thus, the particles of the fine sediment are primarily transported in suspension, and the advection-diffusion equation is used to solve the transport. The erosion flux of cohesive and non-cohesive sediment is taken into account. Three-dimensional morphodynamic models are state-of-the-art, but their practical application is limited due to the long computation time. Therefore, this research attempts to employ a representative wave by the present morphodynamic model in order to investigate the yearly change in the Liaodong Bay. This paper is organized as follows: Section 2 presents governing equations and boundary conditions. Section 3 deals with the validation of the model. Section 4 discusses the results of the practical application. Section 5 concludes the paper.

2 Model description

2.1 Hydrodynamic model

The three-dimensional equations defining the effect of waves are based on the circulation model FVCOM in sigma (σ) coordinates (Chen et al., 2003), where the baroclinic terms are neglected, the horizontal diffusion terms are replaced by the present forms, and the radiation stress terms are added. The vertical accelerations are small with respect to the gravitational acceleration and the vertical momentum equation is reduced to the hydrostatic pressure equation. The hydrodynamic model is written as follows:

$$\frac{\partial \eta}{\partial t}+\frac{\partial (Du)}{\partial x}+\frac{\partial (Dv)}{\partial y}+\frac{\partial w}{\partial \sigma}=0, \tag{1}$$

$$\begin{aligned}&\frac{\partial (uD)}{\partial t}+\frac{\partial (u^2D)}{\partial x}+\frac{\partial (uvD)}{\partial y}+\frac{\partial (uw)}{\partial \sigma}\\ =&fvD-gD\frac{\partial \eta}{\partial x}+\frac{\partial}{\partial x}\left(K_xD\frac{\partial u}{\partial x}\right)\\ &+\frac{\partial}{\partial y}\left(K_yD\frac{\partial u}{\partial y}\right)+\frac{\partial}{\partial \sigma}\left(\frac{K_z}{D}\frac{\partial u}{\partial \sigma}\right)\\ &-\left[\frac{\partial \left(DS_{xx}(\sigma)\right)}{\partial x}+\frac{\partial \left(DS_{xy}(\sigma)\right)}{\partial y}\right],\end{aligned} \tag{2}$$

$$\begin{aligned}&\frac{\partial (vD)}{\partial t}+\frac{\partial (v^2D)}{\partial y}+\frac{\partial (uvD)}{\partial x}+\frac{\partial (vw)}{\partial \sigma}\\ =&-fuD-gD\frac{\partial \eta}{\partial y}+\frac{\partial}{\partial x}\left(K_xD\frac{\partial v}{\partial x}\right)\\ &+\frac{\partial}{\partial y}\left(K_yD\frac{\partial v}{\partial y}\right)+\frac{\partial}{\partial \sigma}\left(\frac{K_z}{D}\frac{\partial v}{\partial \sigma}\right)\\ &-\left[\frac{\partial \left(DS_{yx}(\sigma)\right)}{\partial x}+\frac{\partial \left(DS_{yy}(\sigma)\right)}{\partial y}\right],\end{aligned} \tag{3}$$

where u, v, and w are the velocities in the x, y, and σ directions, respectively; the vertical coordinate σ ranges from $\sigma = 0$ at the free surface to $\sigma = -1$ at the bottom; t is time; η is the free surface elevation; D is the total water depth; f is the Coriolis parameter; g is the gravitational acceleration; and K_x, K_y, and K_z are the mixing coefficients

under waves and currents in the x, y, and σ directions, respectively. In the present study, the mixing coefficients are dependent on the bed shear velocities under waves and currents, which are relevant to the bottom shear stresses. Hence, the horizontal mixing coefficients from Elder (1959) are shown as follows:

$$K_x = K_y = \alpha_x u_* D, \tag{4}$$

where $\alpha_x = 5.93$; u_* is the bed frictional shear velocity due to the combined actions of the waves and currents and $u_* = (2\tau_{cw}/\rho)^{0.5}$, ρ is the water density, and τ_{cw} is the bottom shear stress in a wave-current interaction and is calculated by the nonlinear formula (Soulsby and Clarke, 2005) as follows:

$$\tau_{cw} = \tau_c \left[1 + 1.2 \left(\frac{\tau_w}{\tau_c + \tau_w} \right)^{3.2} \right], \tag{5}$$

where τ_c is the current bottom shear stress and $\tau_c = \left(\tau_{cx}^2 + \tau_{cy}^2\right)^{0.5}$; τ_{cx} and τ_{cy} are the current bottom shear stress components in the x and y directions, respectively; $(\tau_{cx},\ \tau_{cy}) = (\rho\kappa^2 u_c (u_c^2 + v_c^2)^{0.5}/\ln^2(z_1/z_0),\ \rho\kappa^2 v_c (u_c^2 + v_c^2)^{0.5}/\ln^2(z_1/z_0))$, κ is the von Karman constant and $\kappa = 0.4$, z_0 is a bottom roughness parameter, z_1 is the elevation above the bottom; u_c and v_c are the current velocity components in the x and y directions, respectively; τ_w is the wave bottom shear stress and $\tau_w = 0.5\rho f_w u_w^2$, u_w is the near-bed wave orbital velocity and $u_w = \pi H_s/(T \sinh kD)$, T is the wave period; f_w is the wave friction coefficient and $f_w = 1.39(A/z_0)^{-0.52}$, and $A = u_w T/(2\pi)$. The vertical mixing coefficient K_z is assumed to have a parabolic-constant distribution, which gives a better description of the sediment concentration profile in the ocean (van Rijn, 1984). The parabolic-constant distribution of the vertical mixing coefficient is applied to the model and is expressed as follows:

$$K_z = \begin{cases} \kappa u_* z \left(1 - \dfrac{z}{D}\right); & \dfrac{z}{D} \leqslant 0.5 \\ 0.25\kappa u_* D; & \dfrac{z}{D} > 0.5 \end{cases}, \tag{6}$$

where z is the position of water depth.

S_{xx}, S_{xy}, S_{yx}, S_{yy} are depth-dependent radiation stress tensor components derived from Mellor (2008), and are shown as follows:

$$S_{xx} = kE \left(\frac{k_x k_x}{k^2} \frac{\cosh kD(1+\sigma)\cosh kD(1+\sigma)}{\sinh kD \cosh kD} - \frac{\sinh kD(1+\sigma)\sinh kD(1+\sigma)}{\sinh kD \cosh kD} \right) + E_D, \tag{7}$$

$$S_{xy} = S_{yx} = kE \left(\frac{k_x k_y}{k^2} \frac{\cosh kD(1+\sigma)\cosh kD(1+\sigma)}{\sinh kD \cosh kD} \right), \tag{8}$$

$$S_{yy} = kE \left(\frac{k_y k_y}{k^2} \frac{\cosh kD(1+\sigma)\cosh kD(1+\sigma)}{\sinh kD \cosh kD} - \frac{\sinh kD(1+\sigma)\sinh kD(1+\sigma)}{\sinh kD \cosh kD} \right) + E_D, \tag{9}$$

where k is the wave number; k_x and k_y are the wave number components in the x and y directions, respectively; E is the wave energy computed by $E = gH_s^2/8$, H_s is the significant wave height; and E_D is a modified Dirac delta function expressed as follows:

$$E_D = 0, \text{ if } \sigma \neq 0 \text{ and } \int_{-1}^{0} E_D D \mathrm{d}\sigma = \frac{E}{2}. \tag{10}$$

2.2 The representative wave

The relationship between waves and sediment transport is nonlinear and dependent on physical processes. The effective constant wave height will produce the same result as the actual time-varying wave height changes. In this study, the longshore sediment transport process is used to predict the morphological change in coastal zones. Considering that the longshore transport is proportional to $H^{5/2}$ (Steijn and Hartsuiker, 1992), the representative wave height H_{cs} is computed as follows:

$$H_{cs} = \left(\sum_i p_i H_i^{5/2} \right)^{2/5}, \tag{11}$$

where p_i is the occurrence probability of the wave height H_i.

The representative wave height is a result of the contributions of each wave category encountered throughout the year. This representative wave will be applied to the model, and the wave propagating in the domain will be computed by the wave model, i.e., Simulating Waves in the Nearshore (SWAN), which is based on the phase-averaged equation, including source terms, and solves the equation by wave action density. The model represents the effects of spatial propagation, refraction, shoaling, and wave breaking interactions. More details are given by Holthuijsen et al. (2011).

2.3 Suspended sediment transport

The suspended sediment transport is solved by the

advection and diffusion equation, and is shown as follows:

$$\frac{\partial(DC)}{\partial t}+\frac{\partial(uDC)}{\partial x}+\frac{\partial(vDC)}{\partial y}+\frac{\partial(w-w_0)C}{\partial\sigma}$$
$$=\frac{\partial}{\partial x}\left(\lambda_x D\frac{\partial C}{\partial x}\right)+\frac{\partial}{\partial y}\left(\lambda_y D\frac{\partial C}{\partial y}\right)+\frac{\partial}{\partial\sigma}\left(\frac{\lambda_z\partial C}{D\,\partial\sigma}\right), \quad (12)$$

where C is the sediment concentration; w_0 is the settling velocity of sediment particles, and is calculated by the formula $w_0 = KC^{4/3}$; K is an empirical constant and equal to approximately 0.001 depending on the type of sediment (Krone, 1962); and λ_x, λ_y, and λ_z are the horizontal (x, y) and vertical (σ) sediment mixing coefficients, respectively. The sediment mixing coefficients under waves and currents are equal to the flow mixing coefficients in the present study, i.e., $\lambda_x = \lambda_y = K_x$, and $\lambda_z = K_z$.

2.4 Morphological change

The morphological change accounts for cohesive and non-cohesive fractions, and is calculated by the following equation:

$$\rho_0(\varphi-1)\frac{\partial z_b}{\partial t}=F_m+F_s, \quad (13)$$

where ρ_0 is the sediment density; φ is the porosity of the bed material and $\varphi = 0.6$; z_b is the position of the seabed surface; and F_m and F_s are the net flux of cohesive and non-cohesive sediment, respectively.

The net sediment flux at the bottom is related to the quantity of sediment entering the flow due to the erosion flux and the quantity of sediment dropping out of the flow due to the deposition flux. Thus, for cohesive sediment, the net flux $F_m = D_m - E_m$. The deposition flux D_m was calculated by Krone (1962) and the erosion flux E_m was parameterized by Ariathurai and Arulanandan (1978). For non-cohesive sediment, the net flux $F_s = D_s - E_s$.

$$F_m=\begin{cases}E_{01}(1-\varphi)\left(\dfrac{\tau_{cw}}{\tau_e}-1\right) & \tau_{cw}>\tau_e\\ 0 & \tau_d\leqslant\tau_{cw}\leqslant\tau_e\\ \left(\dfrac{\tau_{cw}}{\tau_d}-1\right)w_0C & \tau_{cw}<\tau_d\end{cases}, \quad (14)$$

$$F_s=\begin{cases}w_0C_a & \tau_{cw}\geqslant\tau_e\\ -w_0C & \tau_{cw}<\tau_e\end{cases}, \quad (15)$$

where E_{01} is an empirical parameter and depends on the local sediment and bed conditions. Given that the local sediment is comprised of the fine sediment with a median diameter of 0.0157 mm and the seabed is well-consolidated, it is taken as $5.0 \times 10^{-4}\,\mathrm{kg\cdot m^{-2}\cdot s^{-1}}$ given the variation of the sediment concentration in the Liaodong Bay during the calibrated process. The critical shear stress for erosion τ_e is taken as $0.15\,\mathrm{N\cdot m^{-2}}$; the critical shear stress for deposition τ_d is $0.06\,\mathrm{N\cdot m^{-2}}$; the concentration near the bed C_a is given by the expression $C_a = 0.015 d_{50} T_*^{1.5}/\left(aD_*^{0.3}\right)$, d_{50} is the median diameter and $d_{50} = 0.0157$ mm, a is the reference height, T_* is the transport parameter, and D_* is the dimensionless diameter. These parameters were calculated by van Rijn (1984).

2.5 Boundary conditions

2.5.1 Surface and bottom conditions

At the free surface, i.e., $\sigma = 0$, the velocity expressions are shown as follows:

$$\frac{K_z}{D}\left(\frac{\partial u}{\partial\sigma},\frac{\partial v}{\partial\sigma}\right)=(0,0), w=0. \quad (16)$$

The vertical sediment flux is zero and the following condition is applied:

$$\frac{\lambda_z}{D}\frac{\partial C}{\partial\sigma}+w_0C=0. \quad (17)$$

At the bottom, i.e., $\sigma = -1$, the velocity expressions are given as follows:

$$\frac{K_z}{D}\left(\frac{\partial u}{\partial\sigma},\frac{\partial v}{\partial\sigma}\right)=(\tau_{cwx},\tau_{cwy}), w=0, \quad (18)$$

where τ_{cwx}, τ_{cwy} are the bottom shear stresses under waves and currents in the x, y directions, respectively. They are calculated by the expression $(\tau_{cwx}, \tau_{cwy}) = (\tau_{cx} + \tau_w, \tau_{cy} + \tau_w)$.

Given that the fine sediment consists of cohesive and non-cohesive content, the net sediment flux at the bottom is calculated by the following condition:

$$\frac{\lambda_z}{D}\frac{\partial C}{\partial\sigma}+w_0C=F_m+F_s. \quad (19)$$

2.5.2 Coastal boundary

The normal velocity along the boundary is zero, and the normal derivatives of sediment concentrations are set to zero.

2.5.3 Open boundary

Main tidal constituents M_2, S_2, K_1, O_1 are combined to provide the time series surface elevation by harmonic analysis of tides at the station Huludao harbor. The sediment concentrations are taken from the measured data at the nearby stations.

3 Application and validation of the model in the Liaodong Bay

3.1 Computational domain

Due to the cutoff of nearby rivers over the past several years, and the discharge from the river in the computational domain was less than 1 $m^3 \cdot s^{-1}$ during periods of flood, and that under most circumstances, there was no runoff during 2009, the runoff from the river is not taken into account. Therefore, the morphodynamic model is used to predict the morphological change without sediment input from the nearby rivers in the coastal waters of the Liaodong Bay.

Figure 1 shows the computational domain in the Liaodong Bay. The easting has a length of 74 km and the northing has a width of 31 km.

The grid resolution in the horizontal domain ranges from 200 m along the shoreline to 2,000 m in the offshore zone. The water depth is divided into 10 sigma layers with a resolution ranging from 0.1 m in the coastal zone to 1.1 m in the offshore area.

The simplified annual wave derived from the observed station (Huludao harbor) with an average water depth of 9.5 m is shown in Table 1, where each category of the highest one-tenth wave has the occurrence probability. It can be calculated that the representative wave $H_{1/10}$ is 0.83 m and the corresponding period is 3.0 s, which is the most frequent period with the dominating direction from the south-west. The distribution of the waves in the domain is computed by SWAN and is combined with the tidal currents to predict the morphological change.

3.2 Validation of the model

There are four stations for measurement of tidal level and seven stations for measurement of tidal current and sediment concentrations in the computational domain. The observations were conducted from November 12th to 13th, 2009 during the neap tide and from November 18th to 19th, 2009 during the spring tide, and were measured every. Six points of the water column at the surface layer, 0.2D, 0.4D, 0.6D, 0.8D and the bottom layer were measured. To calibrate and validate the model, the measurements at stations H1 and H4 (tidal level), and V1, V3, and V5 (tidal current and sediment concentration) were chosen. The simulated results are simultaneously compared with the observed data during the spring and neap tide.

Figure 2 depicts the simulated results and measured data of the tidal level at the two stations. The mean absolute errors during the spring tide are 0.13 m and 0.12 m, while the errors during the neap tide are 0.04 m and 0.06 m. The simulated results show a satisfactory agreement with the measured data. Figure 3 presents the validation of tidal currents between the simulated results and measured data at the three stations. During the spring tide, the mean absolute errors of velocities at stations V1, V3, and V5 are 0.03 m/s, 0.054 m/s, and 0.041 m/s, while the mean absolute errors of the directions at the three stations are 47°, 25°, and 35°. During the neap tide, the corresponding deviations of velocities at the three stations are 0.065 m/s, 0.061 m/s, and 0.057 m/s, and the errors of directions are 28°, 15°, and 16°. The simulated depth-averaged velocities and directions agree with the measured data in both magnitudes and phases. The flow characterizes tidal currents in the Liaodong Bay and the varying process of the flow in the computational domain is captured quite accurately by the model.

To validate the vertical distribution of the currents, the simulated and measured results of the mean maximum

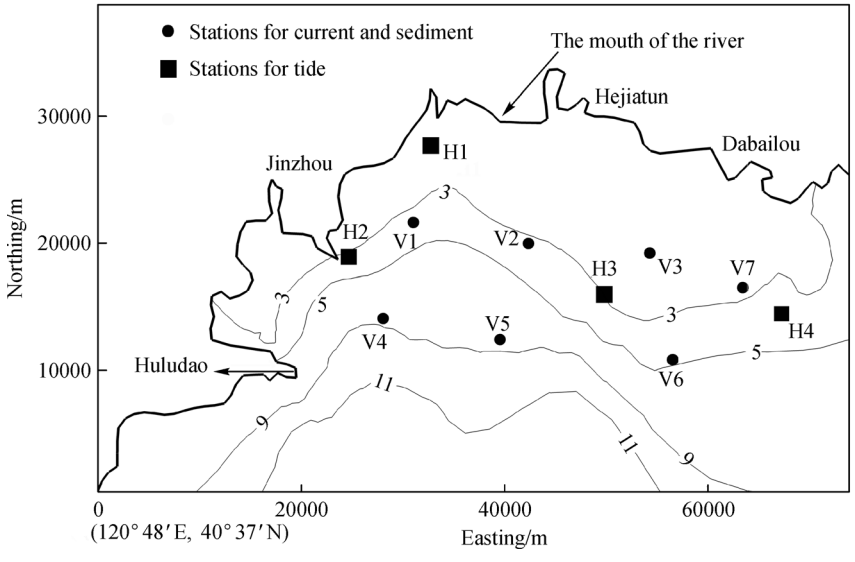

Fig. 1 The water depth and locations of the measured stations in the computational domain.

Table 1 Simplified annual wave

$H_{1/10}$ /m	p_i /%
0.1–0.9	80.32
1.0–1.4	13.01
1.5–2.0	5.95
⩾2.0	0.72

velocity during the spring and neap tide at the three stations are shown in Fig. 4. The mean absolute errors of the velocity during the spring tide at the three stations are 0.015 m/s, 0.013 m/s, and 0.016 m/s, while the errors during the neap tide are 0.014 m/s, 0.012 m/s, and 0.018 m/s. The vertical structure of the currents is non-uniform, and the depth-dependent variation is reproduced by the model. It shows that the vertical distribution of the currents is accurately simulated.

By comparing the tidal level and currents during the observation, the variations of the tidal level and the velocity between the neap tide and spring tide were not noticeable. Therefore, the comparison of the sediment concentrations during the spring tide is carried out.

Sediment transport is computed by two approaches: one accounts for the non-cohesive and cohesive fractions of fine sediment in the present model, and the other takes cohesive sediment into account. The validation of the depth-averaged sediment concentration between the simulated results and measured data at stations V1, V3, andV5 is shown in Fig. 5. The mean absolute errors of the sediment concentrations at the three stations computed by the present model are 0.004 kg/m^3, 0.011 kg/m^3, and 0.012 kg/m^3, while the mean absolute errors of the sediment concentrations accounting for cohesive sediment alone are 0.008 kg/m^3, 0.015 kg/m^3, and 0.014 kg/m^3. Although the difference of the errors is not very noticeable, the present model simulates the variation of the sediment concentration during the tide more accurately than only accounting for cohesive sediment. Meanwhile, it seems that the simulated result is low and deviates from the measured data when only accounting for cohesive sediment. Therefore, it is noticed that the present method accounting for both cohesive and non-cohesive fractions gives a reasonable result of the sediment concentrations in the Liaodong Bay even though there is a slight deviation of phases between the simulated results and the measured data. The overall distributions of the simulated results are in agreement with the measured values.

To validate whether the present model can give an accurate vertical profile of the sediment concentration, the simulated results and measured data of the mean maximum sediment concentration during the spring tide at the three stations are compared and presented in Fig. 6. The mean absolute errors of the vertical sediment concentration at the three stations are 0.006 kg/m^3, 0.004 kg/m^3, and 0.005 kg/m^3. The vertical structure of the sediment concentration shows that the concentration is higher at the bottom than at the surface. The present model thus gives satisfactory predictions of the vertical distribution of the sediment concentration.

The validation demonstrates that the model yields the accurate results of tidal level, velocities, directions, and sediment concentrations. Therefore, the model is applied to predict the morphological change under the representative waves and tidal currents.

4 Results and discussion

4.1 Sediment concentration

The simulated results of the sediment concentration at the surface and bottom layers are shown in Fig. 7. During the flood tide and waves, it is seen that the currents enter the domain from the northeast and flow to the coast. The maximum sediment concentration is 0.15 kg/m^3 at the surface layer and 0.25 kg/m^3 at the bottom layer in the nearshore zone. The high concentration exists around a water depth of 5 m, and the suspended sediment concentration is 0.1–0.15 kg/m^3 at the surface layer, increasing to 0.2–0.25 kg/m^3 at the bottom layer. As the water depth increases into the offshore zone, the sediment

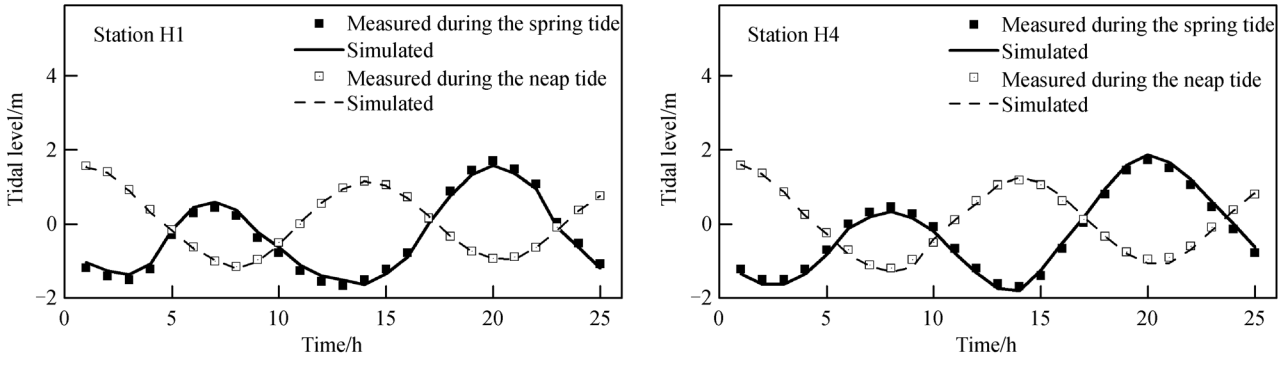

Fig. 2 Validation of tidal level.

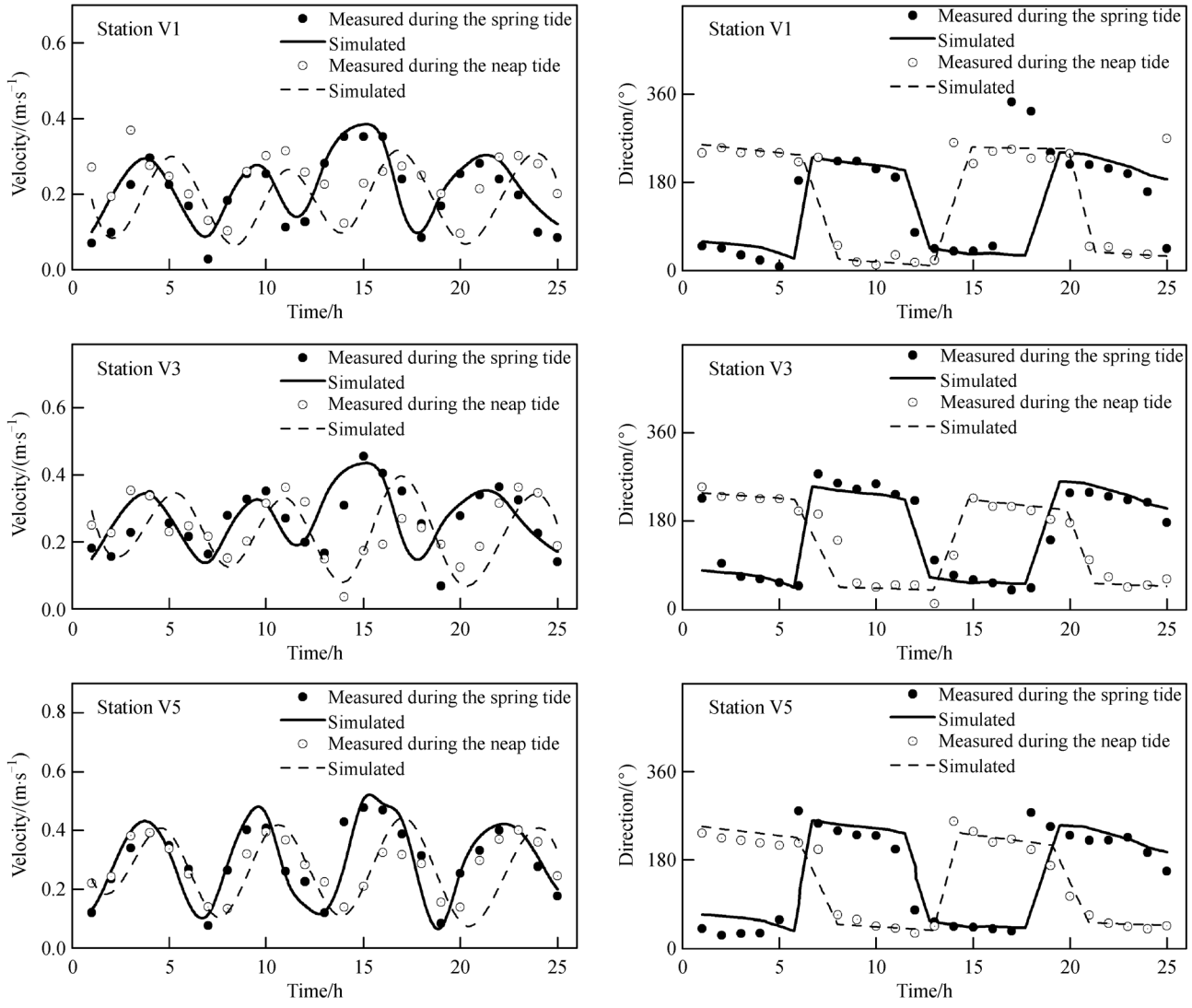

Fig. 3 Validation of current velocity and direction.

concentration decreases to 0.03 kg/m^3 at the surface layer and 0.05 kg/m^3 at the bottom layer. During the ebb tide and waves, the currents flow out of the domain from the southwest, with the distribution of the sediment concentration showing similar characteristics. However, the maximum concentration is more noticeable during the flood tide and waves compared with the result during the ebb tide and waves at the surface layer. Meanwhile, the distribution range of concentrations greater than 0.1 kg/m^3 is wider during the flood tide and waves.

These phenomena can be attributed to the fact that higher current velocities enhance the bottom stresses during the flood tide and waves, and thus can re-suspend more sediment from the seabed. There is a phase-lag between the hydrodynamics and sediment transport (Xie et al., 2010). More sediment in the presence of the enhanced bottom stress is stirred up to enter the flow, and the high concentration is transported to the nearshore zone by the currents. This explains, therefore, the phenomenon of lower sediment concentration in zones with strong currents. In addition, the distribution of the sediment concentration is relevant to the water depth under waves and currents. In the computational domain, there are high sediment concentrations within a water depth contour of 5 m, which increase and reach a maximum within a water depth contour of approximately 3 m under the combined actions of the tidal currents and waves. This could be in relation to the fraction of the local bottom sediment. The non-cohesive sediment is more easily suspended than the cohesive fraction under waves and currents. As a result, higher concentration cores, as seen in Fig. 7, are moved shoreward by the flood tide and seaward by the ebb tide. The flow direction between the surface and bottom layers does not change during the flood or ebb tide and waves, but the velocity is strengthened, and thus, the shoreward transport is enlarged during the flood tide and waves. In

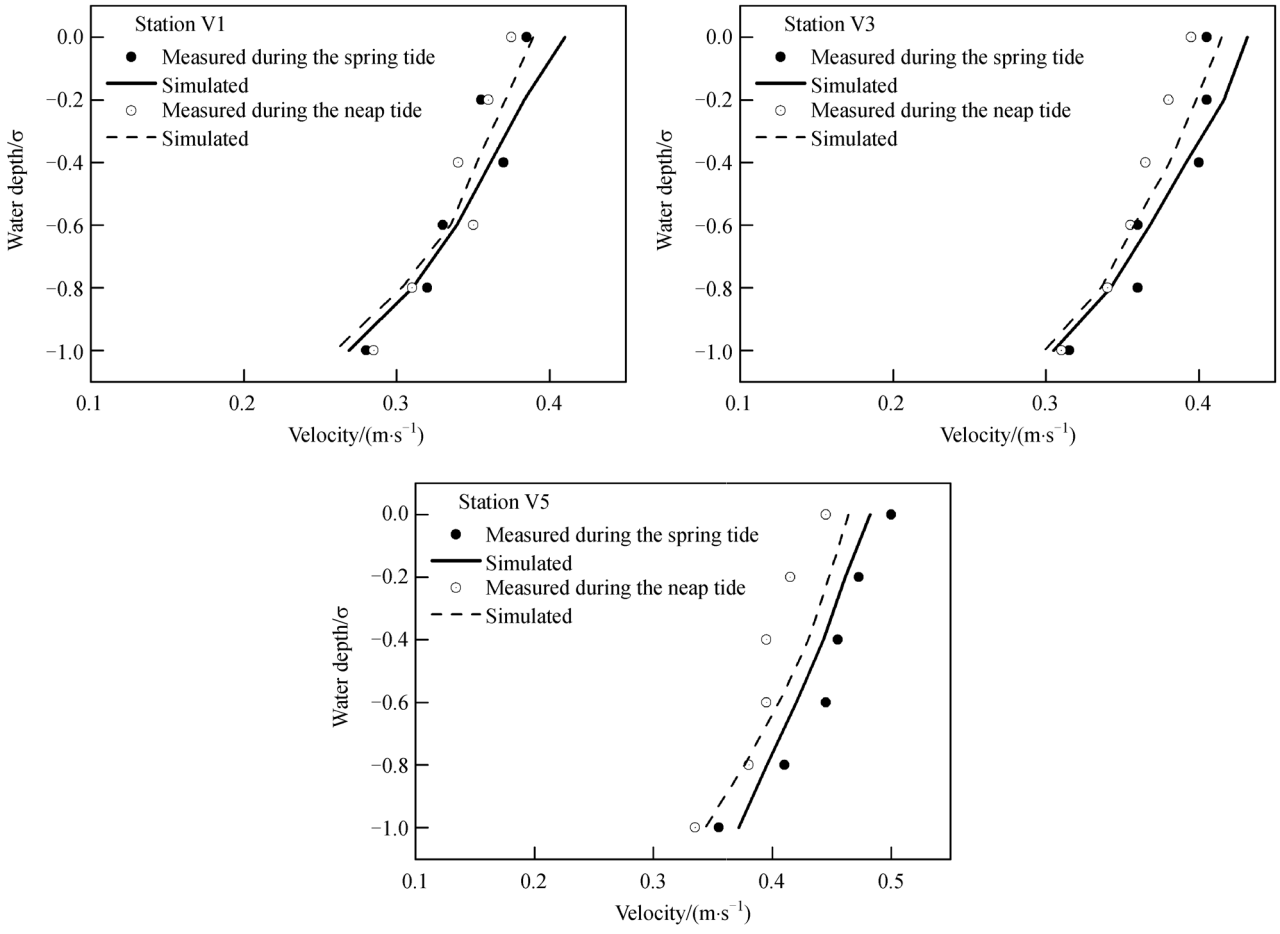

Fig. 4 Validation of the horizontal velocity profiles.

general, the range of the high sediment concentration is broadened, and the distinction between the surface layer and bottom layer is not noticeable. This is mainly attributed to the mixing of the waves and currents so that the suspended sediment can easily diffuse along the water depth.

4.2 Erosion and deposition flux

The annual-averaged erosion and deposition flux of cohesive and non-cohesive fractions is presented in Fig. 8. It is noted that the erosion and deposition flux has larger values within a water depth contour of 5 m, and the quantity of the annual-averaged erosion flux is greater than the absolute quantity of the deposition flux in a water depth contour of 3 m. Meanwhile, the maximum annual-averaged erosion and deposition flux of the non-cohesive fraction is higher than the cohesive sediment. This could be attributed to the fact that the non-cohesive sediment has a relatively larger settling velocity than the cohesive fraction, which leads to a larger deposition flux. In addition, the non-cohesive sediment enters the flow more easily which results in a larger erosion flux than the cohesive fraction. Despite the larger erosion and deposition flux of the non-cohesive fraction, it can be deduced that the annual net flux of the cohesive sediment exceeds the net flux of the non-cohesive fraction.

4.3 Morphological change

The annual morphological change under the combined actions of the tidal currents and waves is displayed in Fig. 9. It demonstrates that the cohesive sediment contributes to the major change, whereas the morphological change is a result of the cohesive and non-cohesive fractions. The final result shows that sedimentation occurs in the shoreline zone with a maximum deposition thickness of 0.01 m, while the erosion occurs at a water depth contour of approximately 3 m, and when the maximum scour reaches 0.015 m after one year. The erosive sediment is transported toward the shoreline zone by the wave-induced currents and the tidal currents. Hence, the shoreline zone exhibits a phenomenon of sediment deposition. In addition, some of the eroded sediment is transported to the offshore area. The deposition thickness in the offshore zone is relatively small.

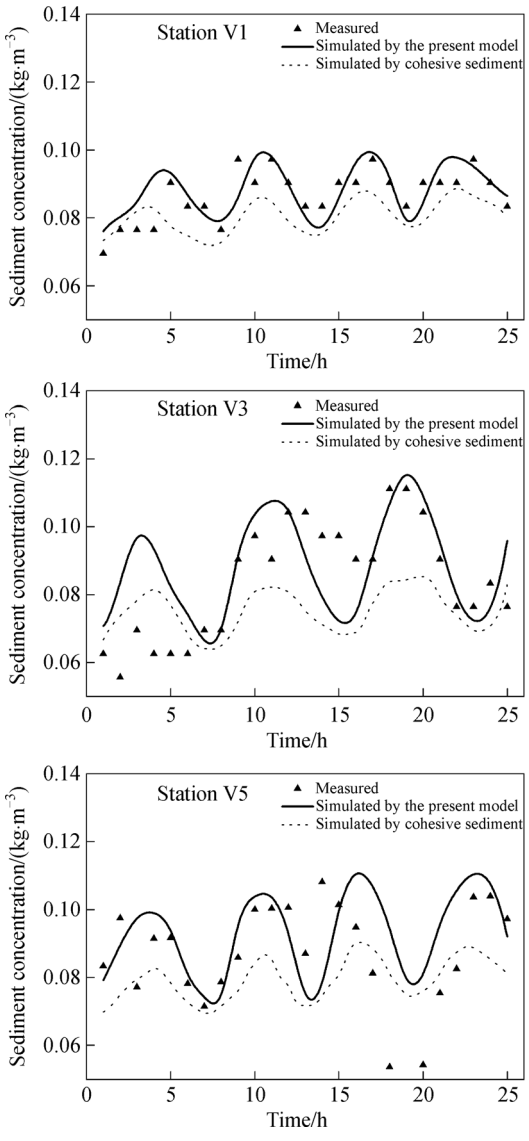

Fig. 5 Validation of sediment concentration.

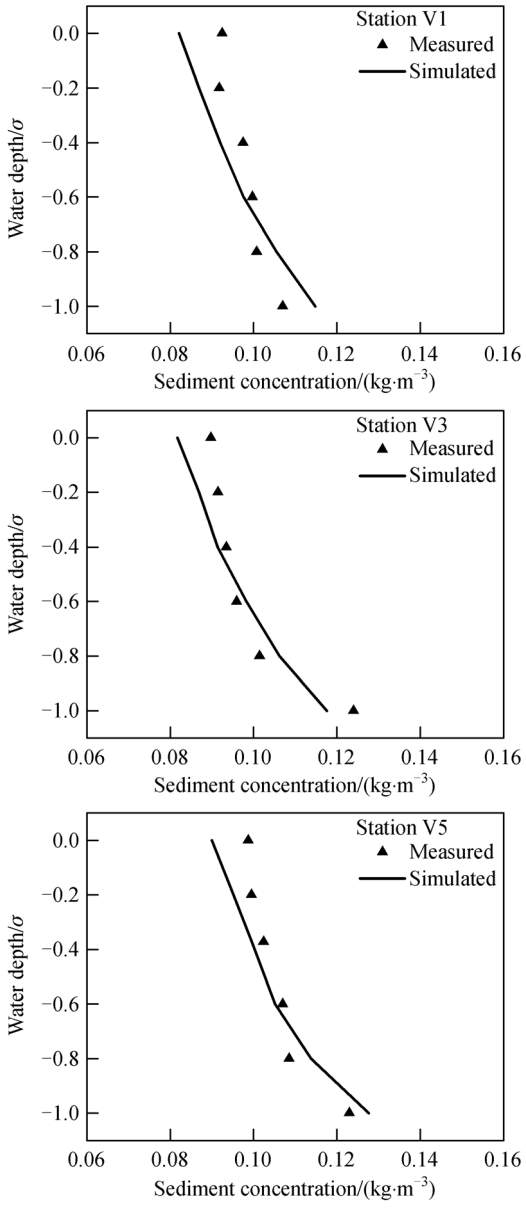

Fig. 6 Validation of the sediment concentration profiles.

From the result of the morphological change without sediment input from the river, the net change in the computational domain is small. The morphology in the Liaodong Bay is in a dynamic equilibrium state, but the erosion is relatively evident due to the cutoff of the rivers. In the study of Wang et al. (2010), the authors concluded that Liaodong Bay had suffered from erosion in recent years based on the change of the shoreline topography. The water depth contour of 5 m had retreated, as compared with the topography during the past ten years. Sedimentation in the shoreline zone was 0.029 m/yr (Wang and He, 1993), while deposition thickness in the nearshore waters was 0.01 m/yr in the present model. It is noted in this study that the sedimentation is decreasing without sediment input from the river. The morphological change is a result of net transport under the waves and currents. Based on the final result of the morphological evolution during one year, it is apparent that future studies should focus on the effects of erosion before the development of coastal construction projects on the seabed.

5 Conclusions

In this study, a three-dimensional morphodynamic model is developed to investigate the morphological change in the Liaodong Bay. The fine sediment transport is resolved by the advection-diffusion equation under the waves and currents. The model accounting for the erosion flux of cohesive and non-cohesive fractions gives a reasonable result when compared to the suspended sediment concentrations. The sediment concentration is significantly

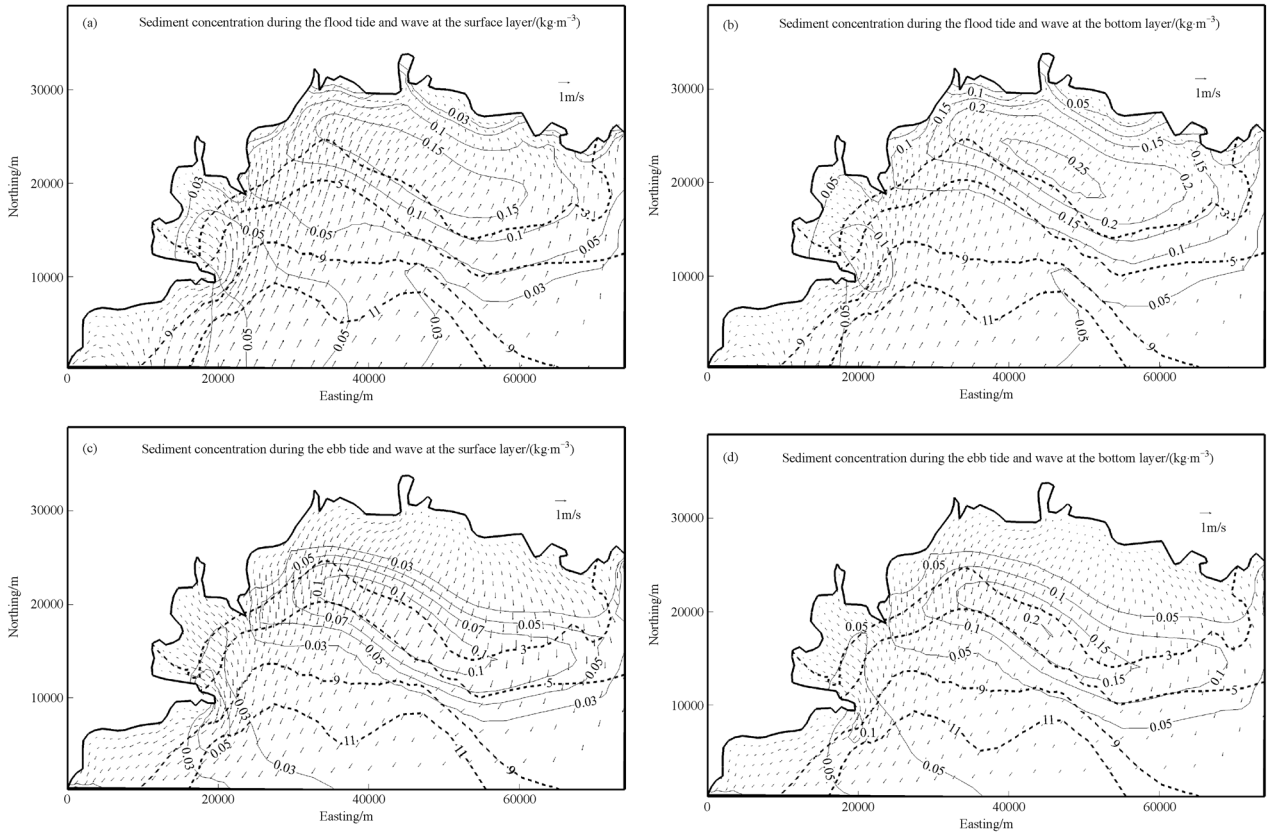

Fig. 7 The distribution of sediment concentration at the surface and bottom layers.

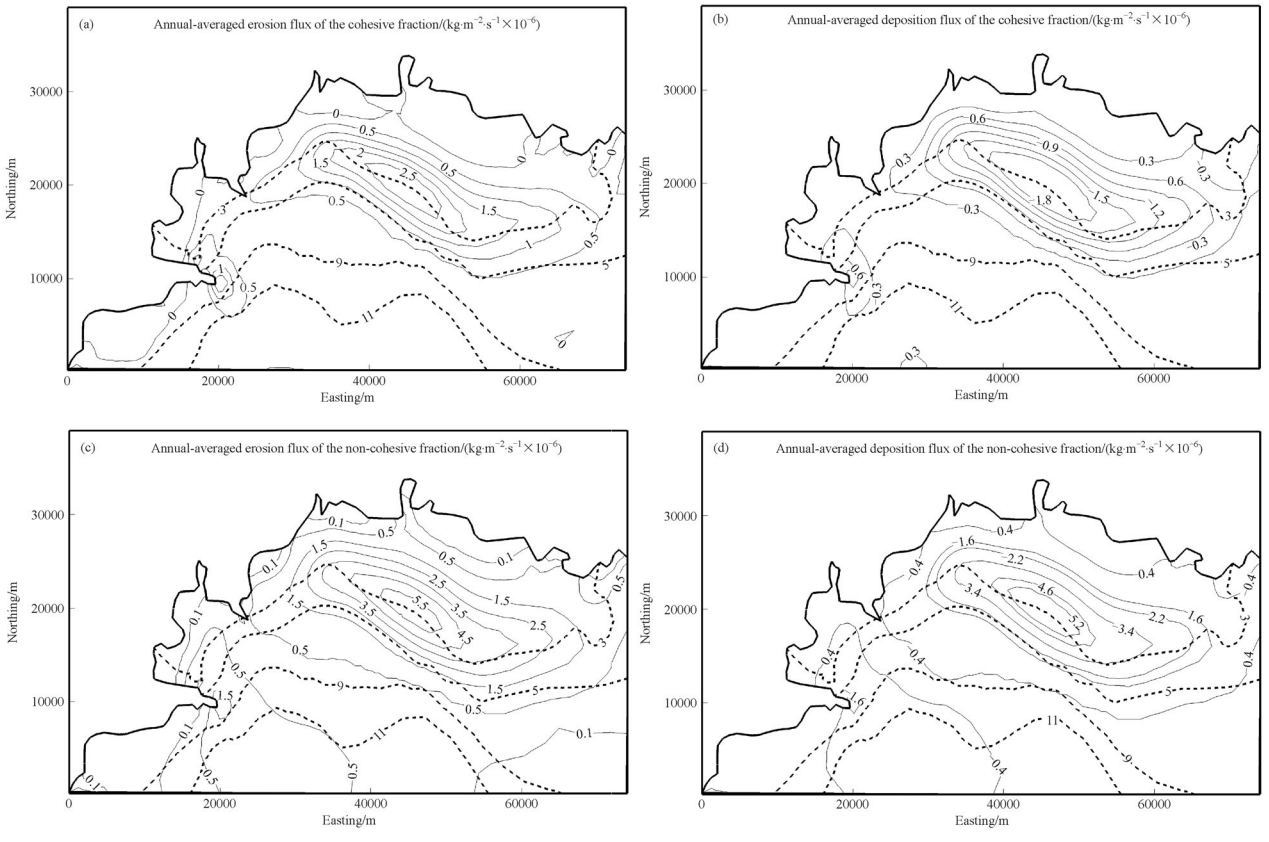

Fig. 8 The distribution of the annual-averaged erosion and deposition flux.

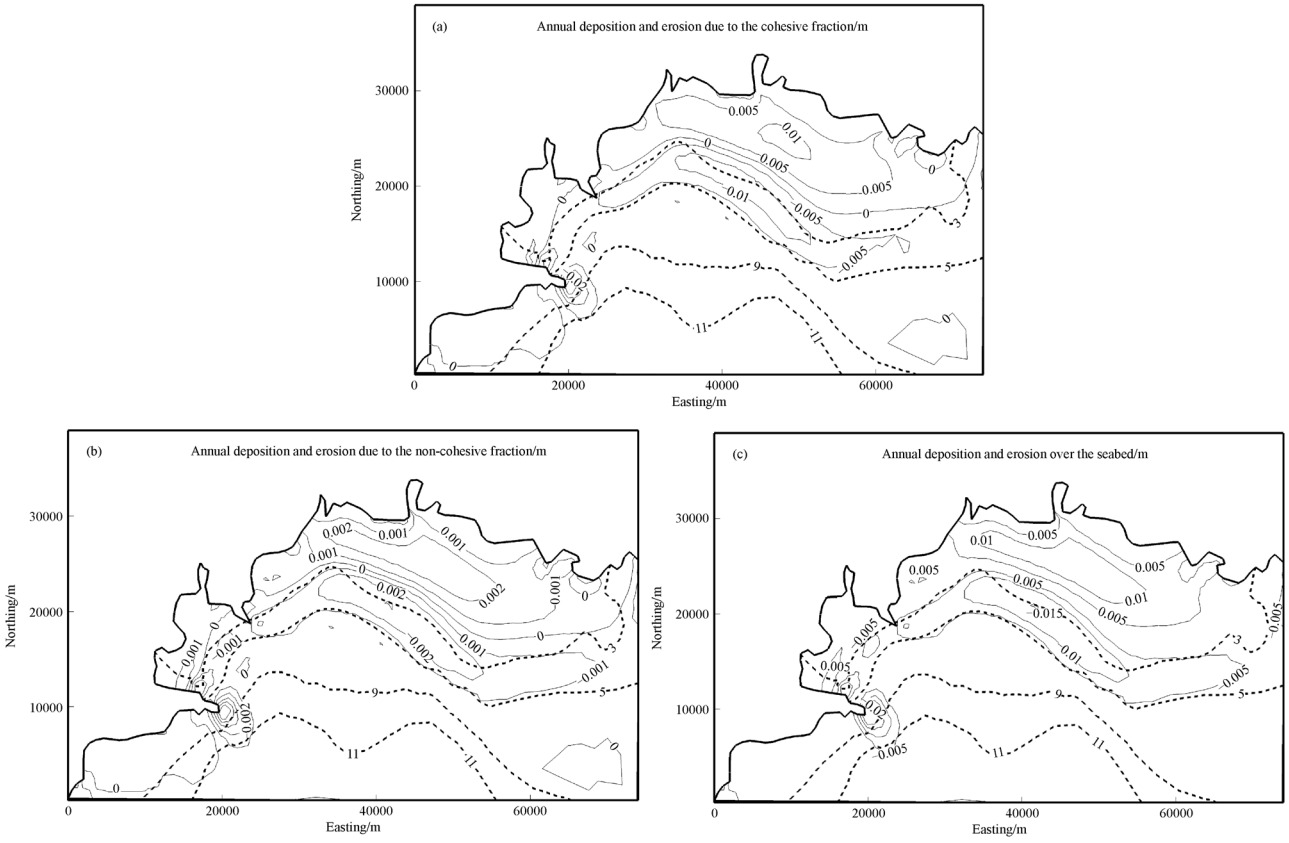

Fig. 9 Morphological changes after one year.

higher in the nearshore area. The simulated morphological change spanning one year is small, but the erosion range is enlarged, when compared with the previous results. Due to the cutoff of the river, the erosion of the morphology is relatively noticeable in the Liaodong Bay. It can be concluded that fine sediment will be transported by the flows and erosion will increase in the absence of sediment input from nearby rivers.

The morphodynamic model, which takes the longshore transport as an annual reference for the representative wave, can reproduce the yearly morphological change. The present approach employing the representative wave instead of real-time wave data saves considerable computation time to predict morphological changes since the wave model is run only once. In practical applications, it is beneficial to employ the representative wave by the morphodynamic model because it reduces the number of calculation loops between the waves and tides. Therefore, the model's use of the representative wave is expected to investigate the long-term morphological evolution in the absence of continuous wave data spanning over a long period. Employing the strategy in the three-dimensional morphodynamic model promises to enhance the study of net change over the seabed.

Acknowledgements The authors appreciate being provided with the source code of the circulation model FVCOM to develop the current work and would thank Jeffrey Steynor and Tsung-Chow Su for revising the original paper. Comments from the anonymous reviewers are acknowledged for improving the manuscript.

References

Ariathurai R, Arulanandan K (1978). Erosion rates of cohesive soils. J Hydraul Div, 104(2): 279–283

Chao X B, Jia Y F, Shields D Jr, Wang S, Cooper C M (2008). Three-dimensional numerical modeling of cohesive sediment transport and wind wave impact in a shallow oxbow lake. Adv Water Resour, 31 (7): 1004–1014

Chen C, Liu H, Beardsley R C (2003). An unstructured grid, finite-volume, three-dimensional, primitive equations ocean model: application to coastal ocean and estuaries. J Atmos Ocean Technol, 20(1): 159–186

Chesher T J, Miles G V (1992). The concept of a single representative wave for use in numerical-models of long-term sediment transport predictions. In: Liu S Q, ed. Hydraulic and Environmental Modeling: Coastal Waters. Brookfield: Ashgate, 371–380

Chonwattana S, Weesakul S, Vongvisessomjai S (2005). 3D modeling of morphological changes using representative waves. Coast Eng J, 47

(4): 205–229

de Vriend H J, Capobianco M, Chesher T, de Swart H E, Latteux B, Stive M J F (1993). Approaches to long-term modeling of coastal morphology—A review. Coast Eng, 21(1–3): 225–269

Du P J, Ding P X, Hu K L (2010). Simulation of three-dimensional cohesive sediment transport in Hangzhou Bay, China. Acta Oceanol Sin, 29(2): 98–106

Elder J W (1959). The dispersion of marked fluid in turbulent shear flow. J Fluid Mech, 5(4): 544–560

Fu W, Li G, Liu G (1994). The hydraulic geomorphological feature and the change of beach face in Jinzhou Bay. Geographical Research, 13 (2): 11–19 (in Chinese)

Holthuijsen L H, Booij N, Ris R C (2011). SWAN user manual (version 40.85). Delft University of Technology Faculty of Civil Engineering and Geoscience Environmental Fluid Mechanics Section

Krone R B (1962). Flume studies of the transport of sediment in estuarial shoaling processes. Final report. Hydraulic Engineering Laboratory and Sanitary Engineering Research Laboratory, Berkeley: University of California: 110

Latteux B (1995). Techniques for long-term morphological simulation under tidal action. Mar Geol, 126(1–4): 129–141

Le Hir P, Cayocca F, Waeles B (2011). Dynamics of sand and mud mixtures: a multiprocess-based modelling strategy. Cont Shelf Res, 31(10): S135–S149

Lesser G R, Roelvink J A, van Kester J, Stelling G S (2004). Development and validation of a three-dimensional morphological model. Coast Eng, 51(8–9): 883–915

Lin B L, Falconer R A (1996). Numerical modelling of three-dimensional suspended sediment for estuarine and coastal waters. J Hydraul Res, 34(4): 435–456

Lopes J F, Dias J M, Dekeyser I (2006). Numerical modelling of cohesive sediments transport in the Ria de Aveiro lagoon, Portugal. J Hydrol (Amst), 319(1–4): 176–198

Mellor G L (2008). The depth-dependent current and wave interaction equations: a revision. J Phys Oceanogr, 38(11): 2587–2596

Miao F, Li S, Li G, Fu W, He B (1996). Suspended sediment transport tendency and the study of sedimentary divisions in the northern Liaodong Bay. Acta Sedimentologica Sinica, 14(4): 114–121 (in Chinese)

Pang C, Yu W (2013). Spatial modes of suspended sediment concentration in surface water in Bohai Sea and their temporal variations. Adv Water Sci, 24(5): 722–727 (in Chinese)

Pinto L, Fortunato A B, Zhang Y, Oliveira A, Sancho F (2012). Development and validation of a three-dimensional morphodynamic modelling system for non-cohesive sediments. Ocean Model, 57 – 58: 1–14

Roelvink J A (2006). Coastal morphodynamic evolution techniques. Coast Eng, 53(2–3): 277–287

Soulsby R L, Clarke S (2005). Bed shear-stresses under combined waves and currents on smooth and rough beds. HR Wallingford, Report TR137

Steijn R C, Hartsuiker G (1992). Morphodynamic response of a tidal inlet after a reduction in basin area. Delft Hydraulics, Coastal Genesis Report, 22–24

van Rijn L C (1984). Sediment transport. 2. Suspended-load transport. J Hydraul Eng, 110(11): 1613–1641

Waeles B, Le Hir P, Lesueur P, Delsinne N (2007). Modelling sand/mud transport and morphodynamics in the seine river mouth (France): an attempt using a process-based approach. Hydrobiologia, 588(1): 69–82

Wang W, Ma H, Yin X, Miao F (2010). Grades and distribution of coastal erosion and siltation in Liaoning Province. Mar Sci, 35(8): 65–68 (in Chinese)

Wang Y and He B (1993). Modern erosion and accumulation trends of the north shallow region of Liaodong Bay. Transactions of Oceanology and Limnology, 15(4): 13–19 (in Chinese)

Warner J C, Sherwood C R, Signell R P, Harris C K, Arango H G (2008). Development of a three-dimensional, regional, coupled wave, current, and sediment-transport model. Comput Geosci, 34(10): 1284–1306

Xie M X, Zhang W, Guo W J (2010). A validation concept for cohesive sediment transport model and application on Lianyungang harbor, China. Coast Eng, 57(6): 585–596

Zhang M, Feng X, Hao Y (2011). Quantitative remote sensing study on spatio-temporal variation of suspended sediment in north Liaodong Bay. J Sediment Res, 56(4): 15–21 (in Chinese)